ACS APPLIED MATERIALS & INTERFACES

Research Article

www.acsami.org

Mesoporous Silica-Layered Biopolymer Hybrid Nanofibrous Scaffold: A Novel Nanobiomatrix Platform for Therapeutics Delivery and Bone Regeneration

Rajendra K. Singh,[†,‡] Guang-Zhen Jin,[†,‡] Chinmaya Mahapatra,[†,‡] Kapil D. Patel,[†,‡] Wojciech Chrzanowski,[‡,§] and Hae-Won Kim*[,†,‡,∥]

[†]Institute of Tissue Regeneration Engineering (ITREN), [‡]Department of Nanobiomedical Science & BK21 PLUS NBM Global Research Center for Regenerative Medicine, and [∥]Department of Biomaterials Science, School of Dentistry, Dankook University, Cheonan 330-714, South Korea

[§]The Faculty of Pharmacy, The University of Sydney, Sydney, New South Wales 2006, Australia

ABSTRACT: Nanoscale scaffolds that characterize high bioactivity and the ability to deliver biomolecules provide a 3D microenvironment that controls and stimulates desired cellular responses and subsequent tissue reaction. Herein novel nanofibrous hybrid scaffolds of polycaprolactone shelled with mesoporous silica (PCL@MS) were developed. In this hybrid system, the silica shell provides an active biointerface, while the 3D nanoscale fibrous structure provides cell-stimulating matrix cues suitable for bone regeneration. The electrospun PCL nanofibers were coated with MS at controlled thicknesses via a sol−gel approach. The MS shell improved surface wettability and ionic reactions, involving substantial formation of bone-like mineral apatite in body-simulated medium. The MS-layered hybrid nanofibers showed a significant improvement in mechanical properties, in terms of both tensile strength and elastic modulus, as well as in nanomechanical surface behavior, which is favorable for hard tissue repair. Attachment, growth, and proliferation of rat mesenchymal stem cells were significantly improved on the hybrid scaffolds, and their osteogenic differentiation and subsequent mineralization were highly up-regulated by the hybrid scaffolds. Furthermore, the mesoporous surface of the hybrid scaffolds enabled the loading of a series of bioactive molecules, including small drugs and proteins at high levels. The release of these molecules was sustainable over a long-term period, indicating the capability of the hybrid scaffolds to deliver therapeutic molecules. Taken together, the multifunctional hybrid nanofibrous scaffolds are considered to be promising therapeutic platforms for stimulating stem cells and for the repair and regeneration of bone.

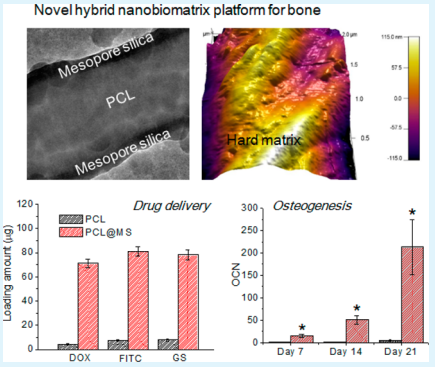

KEYWORDS: *hybrid scaffolds, nanoscale matrix, mesoporous surface, bioactive interface, bone regeneration, drug delivery*

1. INTRODUCTION

Nanoscale substrates and matrices have immense impact on cell behaviors, such as initial adhesion, spreading, mitosis, and lineage-specific differentiation. In the nanomatrix regime, the nanofibrous scaffolds have gained unprecedented attention due to their structural feature that largely mimics the proteineous native extracellular cellular matrix (ECM) of a range of tissues, including skin, muscle, blood vessels, cartilage, nerves, and bone.[1−3] While the nanofibrous matrices hold great merit in terms of topological feature, the surface properties of the matrices critically determine the cellular fate. The lack of adhesive and/or therapeutic motifs largely limits reactions of the matrix with, in the first place, biomolecules (i.e., proteins) and then cells. This reactivity is required to induce rapid tissue healing and repair.[4−6]

It is thus logical that by tailoring the interfacial properties of the nanofibrous scaffolds it would be possible to communicate with cells more effectively and then enhance the tissue regeneration process. A common method to improve the surface reactivity of the polymeric surfaces is to coat them with hydrophilic and natural polymers.[7,8] The interface can be linked with cell-adhesive molecules, such as fibronectin, vitronectin, and collagen, to enhance the initial cellular events.[9,10] Targeting for bone tissue, the surface of scaffolds needs to be specifically tailored to favor and stimulate bone-associated biological reactions and cellular responses.[11,12] For example, scaffolds immobilized with bone ECM proteins significantly induced stem cell differentiation and bone formation.[13−15] When the surface of scaffolds was tailored to be bone bioactive, the calcium and phosphate ions could be substantially induced to form a bone-mineral-like phase that assists in protein adsorption and cellular anchorage.[13,16,17] Furthermore, when the matrix surface was engineered to have stiffer mechanical properties, the osteoprogenitor or stem cells were better driven to an osteogenic lineage through the mechanical signaling pathways.[18−20]

Received: January 22, 2015
Accepted: March 13, 2015
Published: March 13, 2015

DOI: 10.1021/acsami.5b00692
ACS Appl. Mater. Interfaces 2015, 7, 8088−8098

Along with the tailored surfaces, when scaffolds were explored to have the capacity to load and deliver bioactive molecules such as drugs and growth factors, their ability to control cells and enhance bone tissue formation significantly increases.[21−24] Not only the intrinsic properties of the scaffolds but also the exogenous factors tethered to or incorporated within the scaffolds regulate biological pathways including recruiting stem cells, stimulating angiogenesis, and accelerating osteogenesis and mineralization.[13,25] Importantly, the bioactive molecules should be loaded safely and in sufficient quantities to stimulate wanted therapeutic functions, and the delivery rate of the bioactive molecules should be well controlled and sustainable to support ultimate tissue healing and bone formation.[26,27]

Herein, we report on the development of a novel active and hard biointerface of mesoporous silica (MS) on the nanofibrous biopolymer scaffolds. This approach allows two major advances: (i) the stimulation of desired cellular responses (attachment and differentiation) though nanofiber topological and mechanical cues and (ii) the loading and sustainable release of biomolecule/drug cargo from the mesoporous structure of the interface. To the best of our knowledge, this is the first report on the design of a biointerfaced matrix made of MS-shelled nanofibrous polymeric scaffolds with clear evidence showing the capacity of the scaffolds to stimulate cellular responses and simultaneously to load and deliver bioactive molecules for bone regeneration.

2. EXPERIMENTAL SECTION

2.1. Preparation of Mesoporous Silica Shelled Hybrid Nanofibers. The core nanofiber template comprised of poly(caprolactone) (PCL; MW = 80 000, Sigma-Aldrich) was prepared by electrospinning. The PCL solution was dissolved at 12% in 1,2-dichloroethane/methanol and loaded into a syringe equipped with a 21-gauge needle. Then, the material was electrospun onto a metal collector using a high-voltage power supply set to a voltage of 15 kV with a 10 cm distance and an injection rate of 0.5 mL/h.

To form the silica shell interface on the PCL nanofibers, the nanofibers were first soaked in 2 M NaOH for 4 h, with slight modification of our previous reports.[28,29] This alkaline treatment activates the surface of hydrophobic PCL to be hydrophilic with opened carboxylic groups which can allow the subsequent reaction with silica precursors in aqueous medium. After this, the nanofibers were washed and treated with a silica solution through solution-mediated nucleation and crystallization processes as described previously.[30] In brief, to prepare the silica solution, 200 mL of ethanol, 20 mL of water, 200 mg of cetrimonium bromide (CTAB), and 2.4 mL of ammonia (25%) were mixed to produce a basic solution (pH = 10) at room temperature. The CTAB were used for production of mesoporous silica (MS). Tetraethyl orthosilicate (TEOS) was then dissolved into the solution at a ratio of 1:100 by volume. TEOS was then mixed with (3-aminopropyl)triethoxysilane (APTES) (ratio of 4:1 by volume) and used to prepare aminated MS. The silanization of the PCL nanofibers within each silica solution was carried out by dropwise addition of the solution while stirring gently at 200 rpm. The solutions were decanted, and the silica-shelled PCL nanofibers were washed with ethanol (100 mL × 2), water (100 mL × 3), and again with ethanol (100 mL × 2) and then dried overnight at room temperature. The CTAB template was extracted by immersing the nanofibers in HCl solution (15 mL of 37% HCl mixed with 150 mL ethanol) at room temperature for 24 h.

2.2. Characterization of Nanofibers and Silica Shells. X-ray diffraction (XRD; Rigaku) was used to assess the crystal structure of the hybrid scaffolds. The samples were scanned in the range of the diffraction angle 2θ = 10−60° at a speed of 2°/min with a step width of 0.02° 2θ using Cu Kα1 radiation at 40 kV and 40 mA. Fourier transform infrared spectroscopy (FT-IR; Varian 640-IR) was used to determine the status of the chemical bonds of the samples. Twenty scans were recorded in the ATR-FTIR transmission mode at a wavelength from 2000 to 400 cm^{-1}. The morphology of the hybrid scaffolds was examined using transmission electron microscopy (TEM) with a JEOL-7100, and energy-dispersive spectroscopy (EDS) was also carried out. Thermogravimetric analysis (TGA) determined the thermal properties and weight composition of the samples. The water wetting ability of the nanofibers was examined using a benchtop Phoenix contact angle measurement system (PHX300, SEO, South Korea). One drop of deionized water (2 μL) was automatically dispensed onto the sample surface, and images of the water droplets were recorded for 15 s using a video camera system. The surface contact angles were then measured using the Image XP software. Porosity of the silica shell was measured by N_2 adsorption−desorption measurements (Quadrasorb SI, Quantachrom instruments Ltd., USA). The specific surface area was calculated according to the Brunauer−Emmett−Teller (BET) method, and the pore size distribution was determined using the nonlocal density functional theory (NLDFT) method. The acellular apatite-forming ability of the scaffolds was assessed by soaking the samples in simulated body fluid (SBF).[31] Each scaffold sample was immersed in 10 mL of SBF at a pH of 7.4 at 37 °C for up to 3 days, and the medium was refreshed every day. The formation of the apatite layer was examined using SEM, XRD, and FTIR.

2.3. Tensile Mechanical Properties and Nanomechanical Tests. The mechanical properties of the scaffolds were determined using a tabletop uniaxial testing machine (Instron 5966, USA) with a 500 N load cell. Rectangular samples with dimensions of 60 mm × 10 mm × 0.5 mm (thickness) and a gauge length of 40 mm were used. Samples were loaded at a speed of 10 mm/min, stress−strain curves were recorded, and the following parameters were then calculated: elastic modulus, tensile strength, yield point, and elongation. Five replicate measurements were carried out and then averaged.

The nanomechanical properties (Young's modulus) were examined using nanoindentation with atomic force microscopy (MFP-3D-Bio, AsylumResearch) (AFM). The measurements were conducted using silicon probes (Olympus AC-160). The spring constant of the probes was measured using a thermal method, and the sensitivity of the probes was established through a single indentation into freshly cleaved mica. On average, the spring constant of the probes was ∼48 N/m. The samples were probed in the force mode with a maximum load 20 nN and an approaching speed of 40 nm/sec. For each sample, a minimum of 50 individual indents were done, and Young's modulus was calculated from the approach curve using Hertz's model.

2.4. Biological Studies with Mesenchymal Stem Cells. Rat bone marrow mesenchymal stem cells (MSCs) were harvested from proximal and distal epiphyses excised from the femora and tibiae of adult rats (age 5 weeks, Korean) according to the guidelines approved by the Animal Ethics Committee of Dankook University (No. DKU-12-015) and cultured according to the procedures described in a previous study, with a slight modification. MSCs maintained at the 3−4 passages were used in the following experiments.

Each scaffold sample was placed into each well of a 96-well plate, and a suspension of 0.5 × 10^4 cells was seeded on each sample and cultured with growth medium (a minimum essential medium, 1% penicillin/streptomycin, and 10% fetal bovine serum) for periods from 1 to 5 days. At each culturing time, cell proliferation was measured with the cell counting kit-8 (CCK-8, Dojindo Molecular Technologies, Inc.). A 10 μL aliquot of the CCK-8 solution was added to each sample, and cell viability was determined using a microplate reader (Molecular Devices) to measure the absorbance at 450 nm. Each test was performed on three replicate samples. The cell morphology was subsequently examined using SEM after fixation in paraformaldehyde and dehydration in a graded series of ethanol.[30]

To perform the osteogenic differentiation study, quantitative real-time-polymerase chain reaction (RT-PCR) was carried out. Each sample was placed into each well of a 24-well plate, and a suspension of 5 × 10^4 cells was seeded on each sample and cultured with osteogenic medium (growth medium plus 50 μg/mL ascorbic acid, 10 mM β glycerophosphate, and 100 nM dexamethasone) for various

DOI: 10.1021/acsami.5b00692
ACS Appl. Mater. Interfaces 2015, 7, 8088−8098

periods (from 7 to 21 days). After a culture period of 7, 14, and 21 days, the expression of bone-associated genes, including alkaline phosphatase (ALP), collagen type I (Col I), osteopontin (OPN), and osteocalcin (OCN), was confirmed via quantitative RT-PCR. The first strand cDNA was synthesized from the total RNA (1 μg) using a SuperScript first strand synthesis system for RT-PCR (Invitrogen) according to the manufacturer's instructions. The reaction mixture was produced to up to 50 μL, and real-time PCR was conducted using SYBR GreenER qPCR SuperMix reagents (Invitrogen). The relative transcript quantities were calculated using the ΔΔCt method, with glyceraldehyde 3-phosphate dehydrogenase (GAPDH) as the endogenous reference amplified from the samples. The primer sequences of the genes are summarized in Table 1.

Table 1. Primer Sequences of Bone-Associated Genes Used for Quantitative RT-PCR

gene	primer sequence
ALP	(F) 5′-TGACTGACCCTTCCCTCTCG-3′
	(R) 5′-TCAATCCTGCCTCCTTCCAC-3′
Col I	(F) 5′-AGCAAAGGCAATGCTGAATC-3′
	(R) 5′-TGCCAGATGGTTAGGCTCCT-3′
OPN	(F) 5′-GAGGAGAAGGCGCATTACAG-3′
	(R) 5′-AAACGTCTGCTTGTGTGCTG-3′
OCN	(F) 5′-GGCTTCCAGGACGCCTACA-3′
	(R) 5′-CATGCCCTAAACGGTGGTG-3′
GAPDH	(F) 5′-TGAACGGGAAGCTCACTGG-3′
	(R) 5′-TCCACCACCCTGTTGCTGTA-3′

For the study on cellular mineralization, Alizarin red S (ARS) staining was carried out on the cells. After culture in osteogenic medium for 28 days, the samples were fixed in 10% (v/v) buffered formalin, and the specimens were then subjected to Alizarin red S staining for 30 min according to the manufacturer's instructions. The samples were then visualized under an inverted optical microscope (Olympus, Japan).

2.5. Biomolecule Loading and Release. To assess the ability of the scaffolds to load biomolecules within the mesoporous structure and then release them, cytochrome *c* (cyt C) was used as the model protein molecule. First, cyt C solutions of different concentrations (25−300 μg/mL in PBS) were prepared. Within each solution, 4 mg of each scaffold sample (PCL@MS or PCL) was added and left for 24 h at 37 °C. The amount of cyt C loaded onto the scaffolds was plotted with respect to the cyt C concentration used.

On the basis of the loading study of cyt C, a series of biological molecules with different characteristics including surface charge and size was used to test the loading capacity of the developed scaffolds. The molecules include doxorubicin (DOX), fluorescein isothiocyanate (FITC), and gentamycin sulfate (GS), which are relatively small sized and show different charge properties, i.e., cyt C, GS, and DOX are positively charged, while FITC are negatively charged. For the positively charged molecules, nonaminated PCL@MS was used, while aminated PCL@MS was used for the negatively charged molecules. For detection of the amount of cyt C, DOX, and FITC, a UV−vis spectrophotometer (Biochrom) was used at absorbances of 408, 488, and 492 nm, respectively. In the case of GS, *o*-phthaldialdehyde was used as a derivatizing agent to react with the amino groups of GS to yield chromophoric products, and the reaction was carried out by mixing 1 mL of GS sample in solution with 1 mL of isopropanol and 1 mL of *o*-phthaldialdehyde reagent. The GS concentration was determined by the UV absorbance at 332 nm. The loading test was performed in three replicates for each condition (n = 3).

The release profile of the molecules loaded onto the nanofiber scaffolds was examined using cyt C loaded scaffolds as representative samples. For the release study, each scaffold sample was loaded with cyt C at an initial cyt C concentration of 200 μg/mL. The cyt C loaded scaffold samples were immersed in 1 mL of PBS at 37 °C and incubated for up to 2 weeks. At each time point, supernatant was collected to measure the cyt C released. The medium was refreshed after each test for the next run.

2.6. Statistical Analysis. The data are shown as mean ± 1 standard deviation. The statistical comparisons were made using a Student's *t*-test where $P < 0.05$ was considered as statistically significant.

3. RESULTS

3.1. Morphology and Physico-Chemical Properties of the Hybrid Scaffolds. The morphology of the nanofibrous PCL and PCL@MS scaffolds was investigated via SEM and TEM. The electrospun PCL showed randomly oriented nanofibers with an average diameter of 422 ± 97 nm (Figure 1a). The PCL@MS was prepared by in situ nucleation and growth of a nanosilica layer over the PCL nanofiber scaffolds. The PCL nanofibers after the MS deposition processes were observed via SEM (Figure 1b−d). After the first cycle, a homogeneous MS layer was produced on the surface of the PCL nanofibers (Figure 1b). The image of stretched nanofibers revealed the inner PCL and outer MS layer clearly (Figure 1c). After the second reaction cycle, some precipitated silica nanoparticles were observed around the nanofibers, indicating an excessive coating process (Figure 1d). The thickness of the nanofiber increased from 460 for the first cycle to 530 nm for the second cycle, which corresponded to MS shell thicknesses of from 40 to 75 nm, respectively. The formation of a silica shell with an inner PCL core was revealed by the TEM images (Figure 1e and 1f). The PCL@MS hybrid nanofibers were thermally treated at 600 °C for 5 h to remove the inner PCL core, and the SEM images revealed a hollow MS structure (Figure 1g and 1h).

The chemical composition of the MS shell layer was characterized via EDS attached to TEM. Strong peaks only associated with Si, O, and C elements were observed (Figure 1i), suggesting that the coating layer is a pure silica phase. The XRD patterns of the PCL and PCL@MS nanofibers showed typical PCL peaks[31,33] with broad amorphous silica that overlapped the main PCL peak (Figure 1j). The chemical structure of the nanofibers was also characterized using FTIR (Figure 1k). In addition to the characteristic PCL bands (1733−1725 cm^{-1} for —C═O stretching, 1295−1164 cm^{-1} for −C−O stretching, 1419−1367 cm^{-1} for −C−H bending, and 720 cm^{-1} for $-CH_2$ bending of caprolactone),[34] the main absorption bands associated with Si−OH stretching, Si−O bending, and Si−O−Si bending at 1065, 796, and 450 cm^{-1}, respectively,[30,35] were observed for the hybrid nanofibers (Figure 1k).

The thermal behavior of the samples was evaluated via TGA, and the organic and inorganic contents of the hybrid nanofibers were measured (Figure 1l). When calculated based on the residual weight at 700 °C, the amount of silica in the PCL@MS samples was found to be 21.34 ± 1.09%. The results indicated that the sol−gel reactions successfully formed a uniform layer of silica on the surface of the PCL nanofibers, providing unique interfacial properties to the nanofiber matrices.

Next, we characterized the physico-chemical properties of the developed PCL@MS nanofiber. First, the hydrophilicity was evaluated by measuring the incident contact angle. The water sessile drop deformation and contact angle data with respect to time are presented in Figure 2. For the PCL nanofibers, the contact angle was found to remain at 88 ± 1.6° during a 6 s observation. On the contrary, the sessile water droplets

DOI: 10.1021/acsami.5b00692
ACS Appl. Mater. Interfaces 2015, 7, 8088−8098

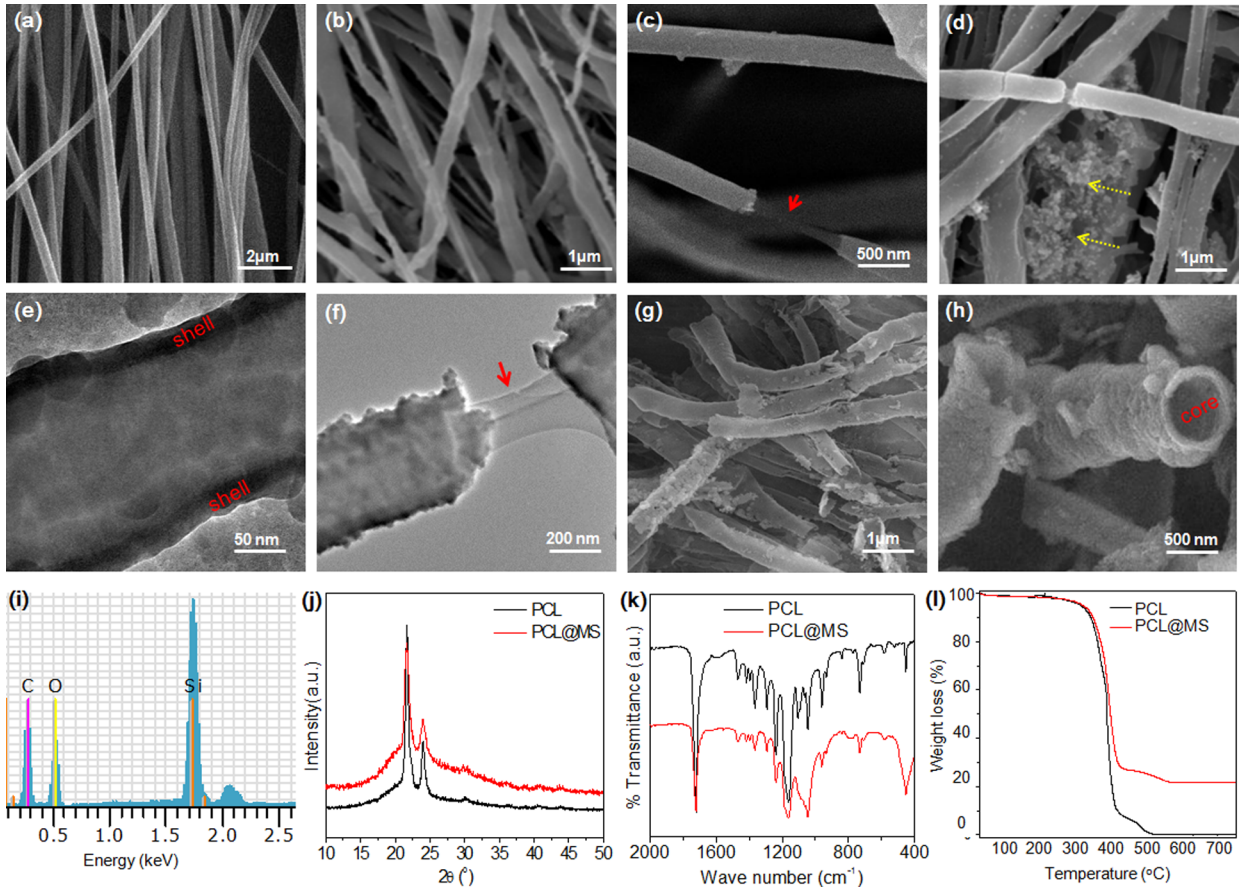

Figure 1. Morphology and characteristics of PCL@MS hybrid nanofibers: (a–d, g, h) SEM and (e, f) TEM images of the samples. (a) PCL used as a template (422 ± 97 nm in size); (b) after 1 coating cycle, PCL@MS induced a homogeneous coverage of the silica layer on the surface; (c) morphology stretched showing the inner PCL (arrow) and outer silica layer; (d) when the coating cycle was exceeded (twice), some precipitates of the silica nanoparticles appear (dotted arrows); (e) TEM image clearly showing the silica layer formed uniformly on the surface (indicated as "shell"); (f) nanofiber stretched revealing the inner PCL (arrow) and the outer silica layer; (g, h) SEM image of the thermally treated PCL@MS, with complete removal of the inner PCL core (indicated as "core"), revealing a hollow MS structure. (i) TEM-attached EDS atomic signals of PCL@MS showing major Si peak development; (j) XRD patterns; (k) FT-IR spectra of the samples. (l) TGA showing weight loss associated with the burn out of organic phases, mainly PCL, and the remaining weight of ∼21.3% that corresponds to the MS layer.

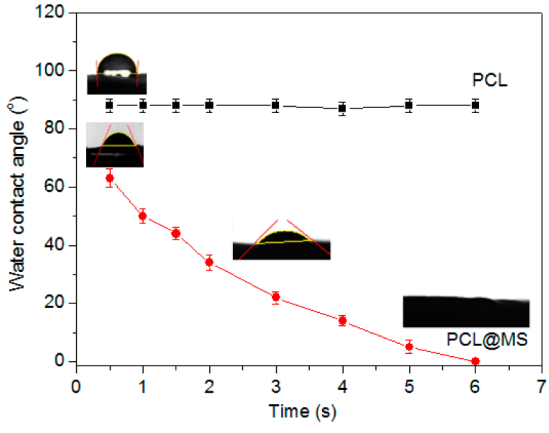

Figure 2. Wettability of the PCL and PCL@MS hybrid nanofibers. Water contact angles with respect to measuring time, showing significant improvement in water affinity of the PCL@MS vs PCL. Representative time frame images of the sessile water drops on the sample shown in inset. Mean ± SD for n = 5.

deformed quickly and spread on the surface of the PCL@MS hybrid nanofibers, showing complete wetting after 6 s.

Since the PCL@MS nanofibers are considered for use as bone regenerative matrices, we investigated the in vitro apatite forming ability in SBF. After only 1 day of immersion in SBF, mineral crystallites were found on the surfaces of the nanofibers and the crystal formation was profound, with thick layering of crystal domains after 3 days (Figure 3a). However, pure PCL did not exhibit any signs of precipitation of the apatite crystals on the surface, suggesting poor bioactivity.

The crystalline phase of the minerals precipitated on the PCL@MS hybrid nanofibers was evaluated via XRD (Figure 3b). Crystalline peaks appeared at 2θ = 26°, 32°, and 41° after soaking in SBF for 1 and 3 days, and these peaks corresponded well with those of the hydroxyapatite (HA) crystalline phase.[31,33] Furthermore, FT-IR analysis showed peaks at 1023 (ν_2), 560 (ν_4), and 600 cm^{-1} (ν_4), which correspond to the PO_4 of the apatite minerals (Figure 3c). These results indicate that the MS-shelled PCL nanofibers were highly reactive, rapidly forming apatite minerals on the surface in SBF, that is, the proposed fibers possess excellent in vitro bone bioactivity. The results were a consequence of the ability of the silanol groups on MS that act as a nucleation site for apatite crystals.

3.2. Mechanical Behaviors. The mechanical properties of the hybrid nanofiber scaffolds were first evaluated via tensile

DOI: 10.1021/acsami.5b00692
ACS Appl. Mater. Interfaces 2015, 7, 8088–8098

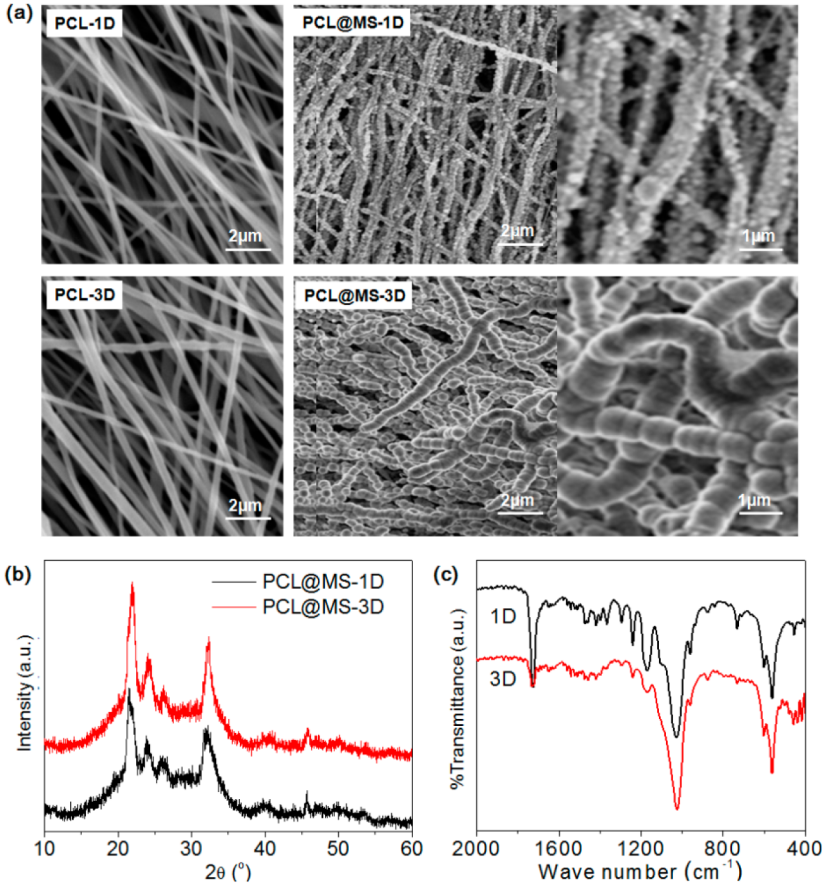

Figure 3. Acellular in vitro bone bioactivity of the nanofiber scaffolds, as assessed by apatite mineralization in SBF during 1 day ("1D") and 3 days ("3D") of immersion. (a) SEM images, (b) XRD pattern, and (c) FT-IR spectrum.

tests. Mechanical properties of the scaffolds was strongly affected by the silica coating on the surface (Figure 4a). The stress−strain curves provide important mechanical parameters, including the tensile strength, stress at yield, elastic modulus, strain at failure, and strain at yield (Figure 4b−f). The PCL@MS hybrid scaffolds showed significantly higher tensile strength (25.4 MPa) than pure PCL scaffolds (10.3 MPa) (Figure 4b), and the yield strength of the hybrid nanofibers was almost double that of pure PCL (15.2 MPa vs 8.01 MPa) (Figure 4c). The elastic modulus of the nanofibers, representing the stiffness of samples, was calculated from the linear region (elastic) of the stress−strain curves (Figure 4d). A marked increase from 48.2 MPa in pure PCL to 125.5 MPa in the hybrid scaffolds was also observed. On the other hand, the elongation of the hybrid scaffolds was substantially reduced from 55% for pure PCL to 14% for PCL@MS in terms of strain at failure (Figure 4e), and from 18% for pure PCL to 2.1% for hybrid scaffolds in terms of strain at yield (Figure 4f).

The nanomechanical properties of the surface of the hybrid scaffolds were further analyzed via nanoindentation. The AFM images show the surface topography of the PCL and PCL@MS nanofiber scaffolds (Figure 5), and the graphs next to the topography images show the force displacement curves of the nanofibers that underwent elastic deformation under force applied by the AFM tip. The force displacement curves for both samples were linear during the loading and unloading cycles. The modulus data was then extracted from the force curves, and the slope of the unloading curve was also calculated. The modulus of the hybrid nanofibers was 64.1 MPa, which was significantly higher than that of PCL 18.3 MPa.

The tensile bulk test and AFM nanosurface test demonstrated that the MS-shelled PCL nanofibers exhibited a significant increase in the strength and stiffness values. In particular, the bulk modulus of the scaffolds and the surface stiffness should be a favorable aspect for use of these nanomatrices in hard tissue regeneration.

3.3. In Vitro Cellular Responses and Osteogenesis. The in vitro cellular responses of the hybrid nanofiber scaffolds were assessed in terms of the cell proliferation and osteogenic differentiation of MSCs. Favorable cell attachment and spreading on the scaffolds is important for subsequent cellular activities. The cell proliferation rate during culture for up to 5 days was significantly higher on the hybrid scaffolds than on pure PCL (Figure 6a). The cell morphology on the scaffolds at day 7 showed actively proliferated cells on both types of nanofiber scaffolds (Figure 6b).

To further evaluate the osteogenic differentiation of the MSCs on the nanofibrous scaffolds, we performed quantitative RT-PCR. The mRNA expression of ALP, Col 1, OPN, and OCN, which are essential osteogenic markers, was analyzed for up to 21 days (Figure 7a). Relative to pure PCL scaffolds, the hybrid scaffolds showed significantly stimulated gene expression levels. While the ALP and Col I genes were stimulated to the highest level at day 14, the OPN and OCN genes were the highest at day 21, indicating time-dependent gene expressions. In particular, the expression of the OCN gene, which is known as a mature osteogenic marker, was as high as 200 times at day

DOI: 10.1021/acsami.5b00692
ACS Appl. Mater. Interfaces 2015, 7, 8088−8098

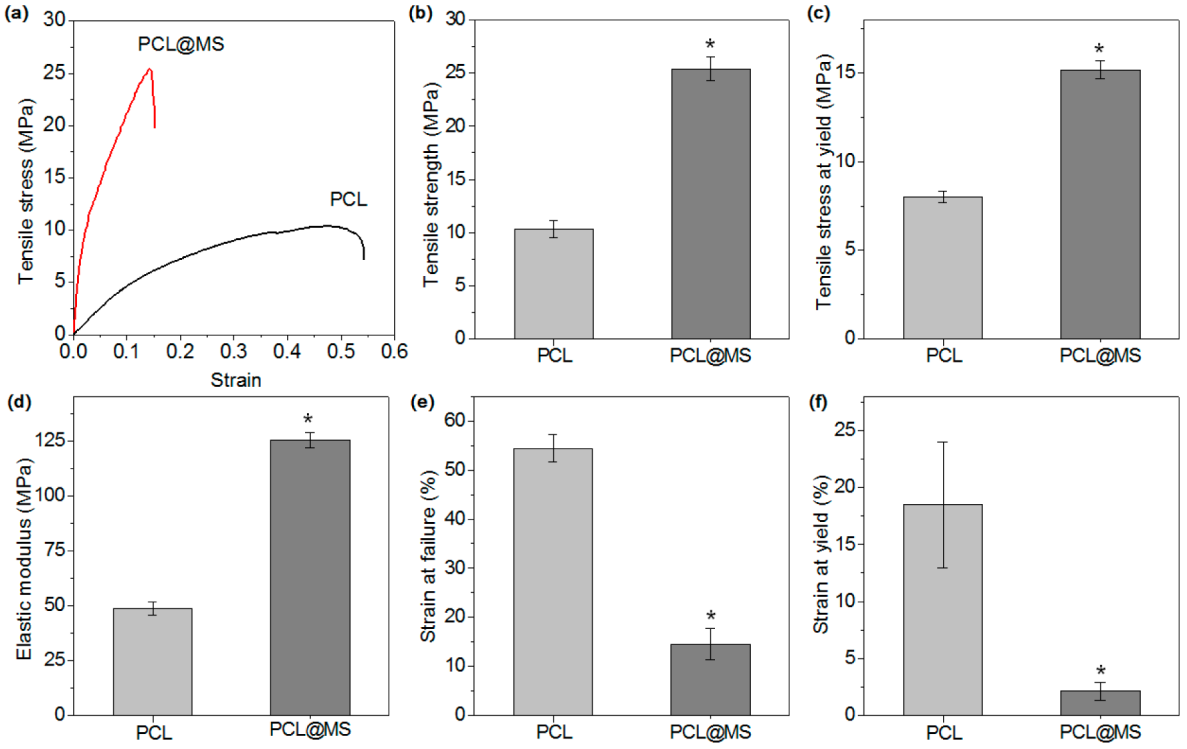

Figure 4. Mechanical properties of the PCL and PCL@MS hybrid nanofibers. (a) Representative tensile stress−strain curves, which were used for the calculation of the mechanical properties, including (b) tensile strength (maximum stress prior to failure), (c) yield strength (tensile stress at yield point), (d) elastic modulus (initial slope), (e) strain at failure (or elongation rate), and (f) strain at yield. Mean ± SD for $n = 5$. Statistical significance noticed between scaffold groups ($^*P < 0.05$).

21. On the basis of this observation, we next assessed the mineralization behavior of the cells at day 28, a period considered to secrete mineral products. The ARS staining images of the samples revealed dark red nodular aggregates of mineralized cells throughout the surface of the hybrid scaffolds which, however, were not readily seen in the pure PCL samples (Figure 7b).

3.4. Mesoporosity and the Capacity of Drug Loading and Delivery. Since the MS-shelled PCL scaffolds are expected to have a high surface area as a result of the possible formation of a mesoporous structure, we analyzed the mesoporosity of the scaffolds. The mesoporosity is considered to be ultimately useful for loading bioactive molecules. Furthermore, we also tailored the nanofiber scaffolds with amine groups in order to functionalize their surfaces. The FT-IR spectra revealed amine groups present on the aminated hybrids scaffolds (Figure 8a, as indicated by arrows). This switchable charge characteristic of the hybrid scaffolds, afforded by a simple surface treatment, should allow for the versatile loading of biomolecules over a broad range, from negatively to positively charged ones, through charge−charge interactions.

The effects of the MS shells on the mesoporosity were further characterized via BET (Figure 8b). The nitrogen adsorption/desorption isotherm curve of the hybrid scaffolds represents a behavior typical of mesoporous materials, with a sharp upturn in the high relative pressure region, which, however, was not readily observed in the pure PCL scaffolds. The average pore size, specific pore volume, and specific surface area values were also presented (Table 2).

The surface area of the PCL@MS nanofiber was significantly higher (224 $m^2\ g^{-1}$) than that of PCL nanofiber (10 $m^2\ g^{-1}$), an increase of as high as 22 times. The specific surface area values of the MS-shelled samples were relatively high, varying from 224 $m^2\ g^{-1}$ for the bare hybrid scaffolds to 198 $m^2\ g^{-1}$ for the aminated scaffolds. In parallel, the pore volumes were very high, varying from 0.47 to 0.44 $cm^3\ g^{-1}$. The mesopores generated in the hybrid scaffolds were distributed over a narrow range (Figure 8c) with average values of approximately 2.5−2.7 nm. The BET results indicate that the MS coating endowed the PCL scaffolds with a high level of mesoporosity, which provides great potential for loading small therapeutic molecules.

The drug loading and release capacity of the developed PCL@MS hybrids scaffolds was studied by selecting four types of biomolecules, including cyt C, DOX, GS, and FITC. These biomolecules have sizes that are suitable for loading onto mesopores while having different surface charge properties, i.e., cyt C, GS, and DOX are positively charged, and FITC are negatively charged. Accordingly, the nonaminated (negatively charged) and aminated (positively charged) hybrid PCL@MS scaffolds were selectively used for the oppositely charged drug molecules. First, we tested the loading capacity for cyt C onto the nonaminated hybrid scaffolds by varying the amount of cyt C as a representative molecule (Figure 9a). The adsorption isotherm showed a striking difference in the loading capacity between PCL and PCL@MS hybrid scaffolds, i.e., only ∼7.8 μg for PCL scaffolds vs ∼84.1 μg for hybrid scaffolds. The difference in the loading capacity suggests that the mesoporosity in the MS shell is effective in capturing the cyt C molecules. On the basis of this, we tested the loading capacity of the other molecules by using a fixed concentration of 120 μg/mL, and hybrid nanofibers with different surfaces were used considering the charge interactions. The loading amount for all molecules was significantly higher for the hybrid scaffolds than for pure PCL: 71 vs 4 μg for DOX, 81 vs 7.5 μg

DOI: 10.1021/acsami.5b00692
ACS Appl. Mater. Interfaces 2015, 7, 8088−8098

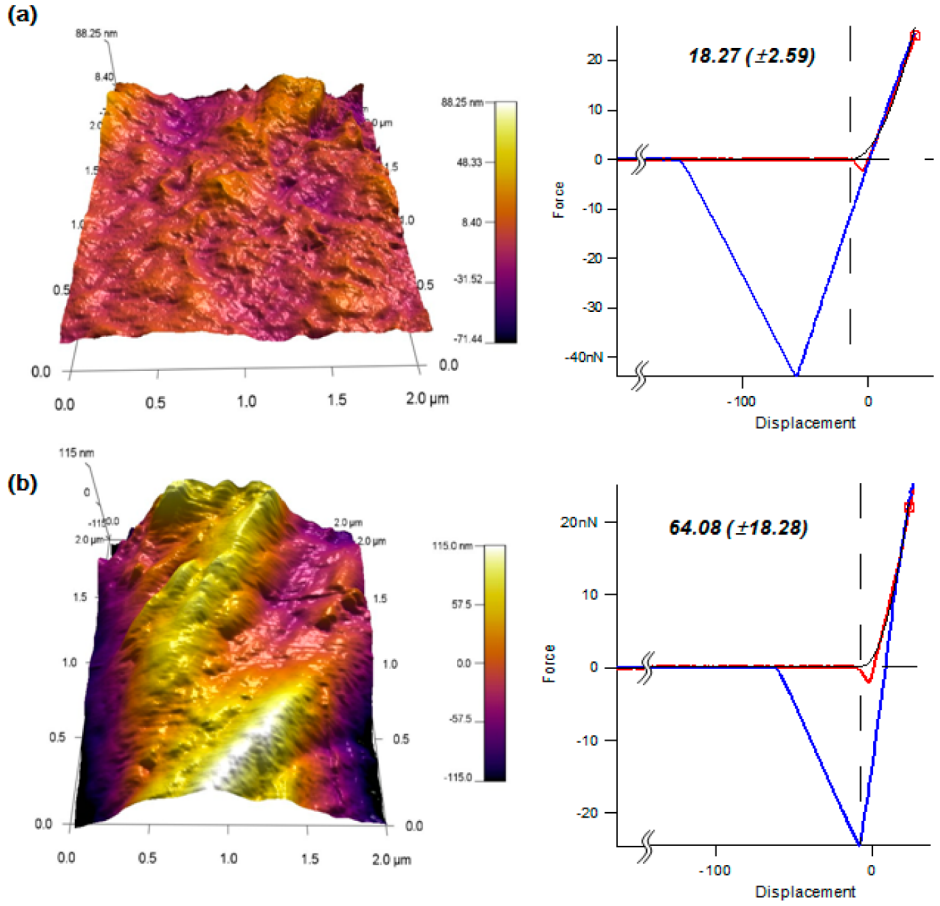

Figure 5. AFM surface topography and nanoindentation graph showing force versus displacement: (a) PCL and (b) PCL@MS.

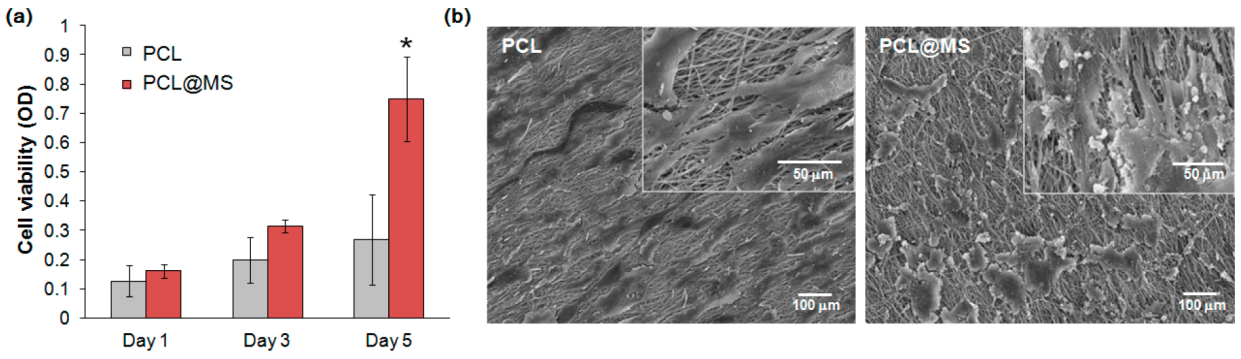

Figure 6. (a) MSC viability measured by CCK assay for up to 5 days. A significantly higher level is shown for PCL@MS than for PCL at day 5 (*P < 0.05, n = 3). (b) SEM cell morphology at day 7. While the cell morphology on PCL@MS appeared to be highly granulated, indicating possible differentiation, cells on pure PCL showed a well-spread morphology.

for FITC, and 78.2 vs 7.8 μg for GS (Figure 9b). The results clearly demonstrate the efficacy of the MS on the surface in taking up various model molecules within the mesopore structure.

Next, we investigated the release profile of the loaded molecules using cyt C as the representative example (Figure 9c). Cyt C was released abruptly from the pure PCL scaffolds, showing a complete release within 24 h. However, the cyt C release from the hybrid scaffolds was very sustainable; after a relatively fast initial release (<10 h) of ~39% of the protein, the release was slowed down and continued over 2 weeks, reaching ~80% of the protein.

4. DISCUSSION

As the scaffolds for cell culture and tissue repair, nanofibrous matrices have shown promising results mainly due to their tissue mimic architecture.[36−42] For the regeneration of hard tissues like bone and tooth structure, bioactive inorganic phases have been attractive through providing chemical and/or physical bone bioactive cues to the cells involved in osteogenic processes. Inorganic nanofibers have poor mechanical stability needing significant improvement to be effectively used as cell-supporting matrices.[43,44] On the other hand, polymeric nanofibers provide adequate structural support, but their surface needs to be improved to favor biological reactions, such as cellular recognition and osteogenesis.[31,45,46] Some

DOI: 10.1021/acsami.5b00692
ACS Appl. Mater. Interfaces 2015, 7, 8088−8098

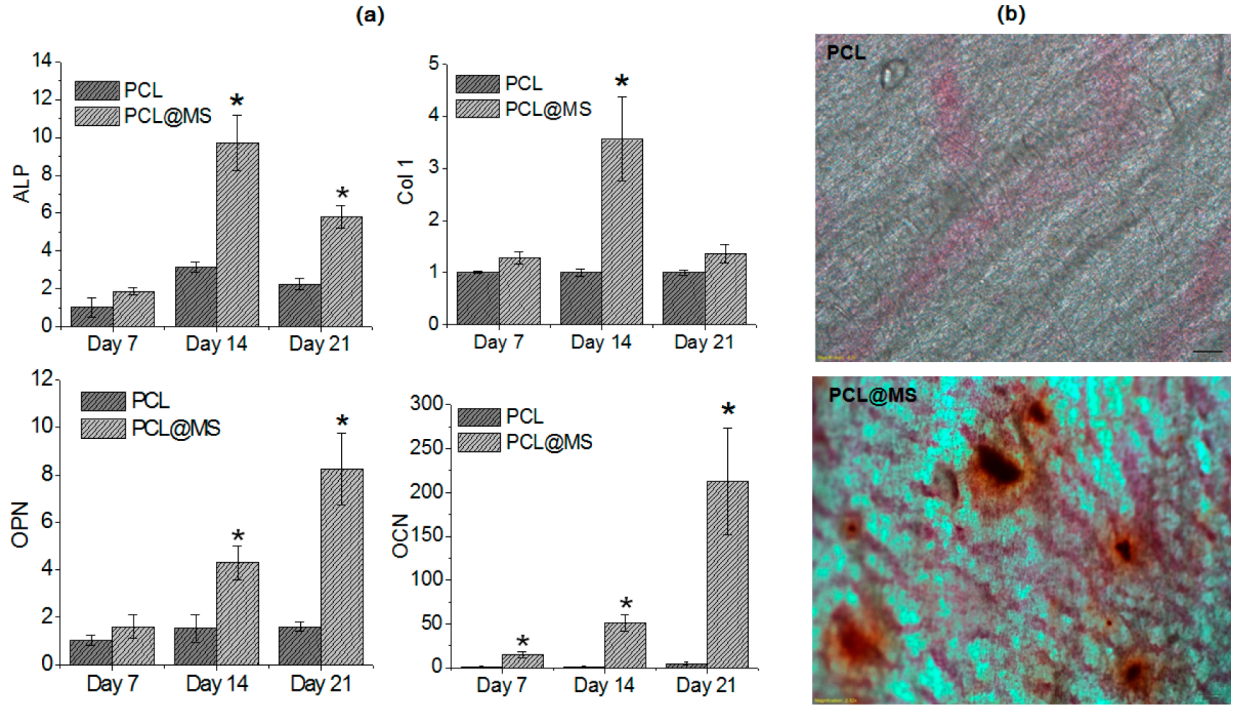

Figure 7. (a) mRNA levels of the osteogenic genes, including alkaline phosphatase (ALP), collagen type I (Col I), osteopontin (OPN), and osteocalcin (OCN), during culture for up to 21 days. Significantly higher gene expressions are shown for PCL@MS (*$P < 0.05$, $n = 3$). (b) Cellular mineralization at 28 days assayed using the ARS staining method (images). Substantial cellular mineralization can be seen for PCL@MS.

studies recently introduced mineralized apatite crystals on the surface and have shown an improvement in the cellular responses.[47,48]

Here we explored the surface of biopolymer nanofibers with a thin MS layer in order to generate organic@inorganic hybrid scaffolds for bone regeneration. While the MS layer was first intended to provide matrix cues favorable for cells to an osteogenic lineage, additional therapeutic functions of the layer were also promised through the delivery of bioactive molecules. For this a series of reactions involving surface activation of PCL and sol−gel silica nucleation and growth processes was introduced, where CTAB was also used as a mesopore generator, which was previously shown to be effective for generating mesoporous silica layering on carbon nanotubes.[49] Through the sol−gel processes a very uniform silica layer with a thickness level of tens of nanometers and a mass fraction of ∼21% could be produced on the PCL nanofiber scaffolds.

The MS layer dramatically changed the physicochemical properties of the PCL surface in a way that presents favorable interfaces for cell culture and hard tissue repair. First, the MS layering enabled the nanofiber scaffolds to have excellent hydrophilicity. In fact, polymer nanofibers, such as those made from PCL, have poor water wettability, and as a result, the initial biological reactions are largely retarded; thus, the superhydrophilic MS-interfaced nanofibers should have the merit of rapid biological reactions, like protein adsorption, which can ultimately improve the subsequent cellular responses.[50,51] Furthermore, the MS-layered surface showed excellent bone bioactivity, exhibiting ultrarapid formation of bone-like mineral apatite crystals in SBF—the coverage of an apatite mineral phase over the entire nanofiber surface occurred within just few days. This was mainly possible due to the presence of a bunch of highly negatively charged silanol groups introduced on the surface, which strongly attract calcium ions followed by subsequent deposition of phosphate ions to form calcium phosphate minerals. Not only the chemical charge effect but also the highly enhanced surface area due to mesoporosity can account for the substantially enhanced surface bone bioactivity of the nanofibers.

One of the most significant and positive changes obtained by formation of the MS layer on nanofibers is the improvement of the mechanical properties. The MS layered on the surface was highly effective in increasing the mechanical strength and the bulk elastic modulus of the polymeric matrices while compensating for the elongation behavior. Furthermore, AFM analysis revealed that the nanoelasticity of the surface was significantly increased after deposition of the MS layer. In fact, polymeric nanofibers like PCL are extremely flexible and provide a matrix more favorable for soft tissues rather than hard tissues. Cell fate is known to be strongly influenced by the stiffness of the matrix.[52] In particular, multipotent stem cells are reported to differentiate into different cell lineages depending on the rigidity of the matrix, i.e., nerve cells are produced on a soft matrix, muscle cells on a medium one, and bone cells on a hard matrix. The multipotent stem cells therefore recognize the flexibility of the underlying matrix and conform to the lineage that has a similarity in stiffness.[52,53] Thus, the increase in modulus due to MS layering provides stiff matrix conditions that might drive stem cells to preferentially commit hard tissue-forming cells.

The gene expressions and cellular mineralization indicated a significant improvement in the in vitro osteogenic differentiation of the MSCs on the MS-surfaced scaffolds. During the culture period of 1−3 weeks, which is considered to span osteogenic differentiation of MSCs, a series of genes, including Col 1, ALP, OPN, and OCN, was significantly upregulated in a time-dependent manner on the MS-shelled matrices. In fact, osteogenic differentiation generally involves temporal mod-

DOI: 10.1021/acsami.5b00692
ACS Appl. Mater. Interfaces 2015, 7, 8088−8098

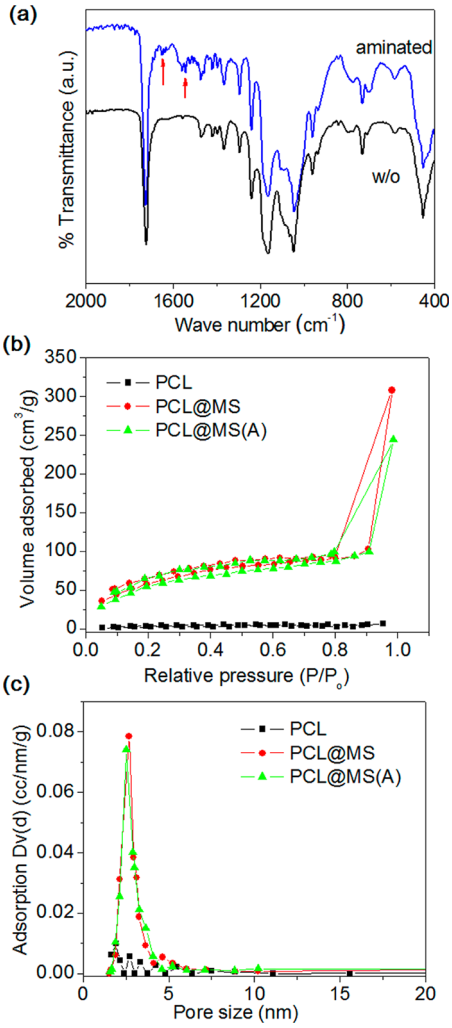

Figure 8. Measurements of the surface mesoporosity of the hybrid nanofibers with (PCL@MS(A)) or without surface amination (PCL@MS). (a) FT-IR spectra revealed amination (arrows assigned to N−H bands). (b) N_2 adsorption/desorption curves, which exhibited the characteristic behaviors of mesoporous materials. (c) Mesopore distribution curves for the hybrid nanofibers.

Table 2. Summary of BET Results with Respect to Mesoporosity, Including Surface Area, Pore Volume, and Mesopore Size

	PCL	PCL@MS	PCL@MS(A)
surface area (m^2/g)	10	224	199
pore volume (cm^3/g)		0.47	0.44
pore size (nm)		2.67	2.51

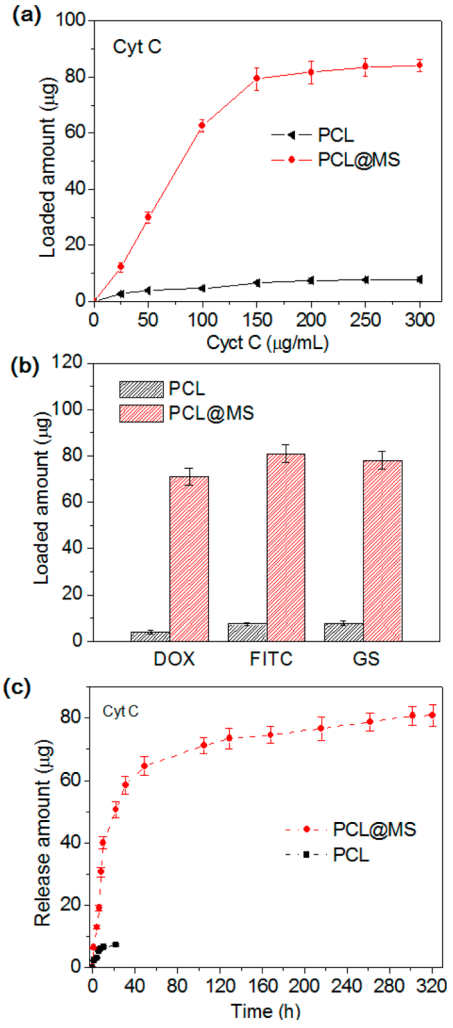

Figure 9. Loading and delivery potential for therapeutic molecules by the hybrid nanofibers. (a) Loading amount onto PCL@MS and PCL of the cyt C model protein, presented according to the cyt C concentration that was initially used. Different cyt C concentrations (from 25 to 300 μg/mL) were used to load onto 4 mg of each scaffold, and the loaded quantity was recorded. (b) Three different model biomolecules, DOX, FITC, and GS, chosen for loading onto each scaffold at a constant initial concentration (120 μg/mL) of the biomolecules. (c) Cyt C release profiles from the scaffolds, recorded in PBS at 37 °C for a period of up to 2 weeks.

ifications in gene expression, which is composed of three gradual steps: proliferation, ECM production and maturation, and matrix mineralization.[54] In this scenario, Col 1 is mostly expressed during the initial proliferative phase and ALP is considered to be a relatively early marker of ECM production.[55] Furthermore, OPN and OCN exhibit a high expression at a later stage of matrix maturation and are involved in mineralization.[56] Our results on gene expression demonstrated a time-sequenced ECM production of cells that are heavily committed to an osteogenic lineage. Although we did not analyze the ECM composition of the cellular products in this study, collagen matrix biosynthesis is principally followed by the expression of osteoblast-specific noncollagenous proteins (such as OPN and OCN), which, together with a phosphate source, wait for subsequent mineralization.[57,58] A substantial level of ARS stains in the nodules distributed throughout the MS-layered scaffolds suggests a possible series of events during ECM production and mineralization.

While the hybrid scaffolds promised an effective role as a matrix for stem cell behavior toward bone, they also showed additional important performance in drug delivering capacity. The MS interfaced on the nanofibers provides a high level of mesoporosity, which allows for small therapeutic molecules to be loaded. Furthermore, the MS surface could be easily modified to exhibit different surface charges, and this ability to alter the charge of the PCL@MS hybrid scaffolds allows versatile biomolecule loading over a broad range, from negatively to positively charged biomolecules, through a charge−charge interaction. The results clearly demonstrated

DOI: 10.1021/acsami.5b00692
ACS Appl. Mater. Interfaces 2015, 7, 8088−8098

the effective role of the MS present on the surface in taking up different model molecules within the mesopore structure at substantially large quantities (10−20 times higher than pure PCL).

Furthermore, subsequent release profiles of the molecules (cyt C herein) loaded onto the hybrid nanofibers were highly sustainable, with ∼39% released during the first 10 h, followed by a slow diffusion-controlled release of over 2 weeks. The release profile shows a striking contrast to the case of pure PCL scaffolds, where the release is abrupt and completed within 24 h. The cyt C molecules that are weakly bound to the PCL nanofiber surface should be easily liberated in the ionic water-based solution. The results of the molecular loading and release of hybrid nanofibers support their future applications for delivery of drugs and protein molecules, to potentiate therapeutic functions of matrices.

In conclusion, the currently developed multifunctional MS-shelled PCL hybrid nanofiber scaffolds have demonstrated excellent properties that are favorable for bone, including in vitro bone bioactivity, mechanical functionality, osteogenic stimulation of stem cells, and the ability to deliver a therapeutic cargo contained in the mesopores over a long period of time. While further studies still remain to determine the bone regenerative ability of the scaffolds in vivo, these findings are considered to promise their potential usefulness as therapeutically relevant nanobiomatrix platforms for the repair and regeneration of bone.

AUTHOR INFORMATION

Corresponding Author

*Tel.: +82 41 550 3081. Fax: +82 41 550 3085. E-mail: kimhw@dku.edu.

Notes

The authors declare no competing financial interest.

ACKNOWLEDGMENTS

This work was supported by the Priority Research Centers Program (No. 2009-0093829) through the National Research Foundation, Republic of Korea.

REFERENCES

(1) Dvir, T.; Timko, B. P.; Kohane, D. S.; Langer, R. Nanotechnological Strategies for Engineering Complex Tissues. *Nat. Nanotechnol.* **2011**, *6*, 13−22.

(2) He, C.; Nie, W.; Feng, W. Engineering of Biomimetic Nanofibrous Matrices for Drug Delivery and Tissue Engineering. *J. Mater. Chem. B* **2014**, *2*, 7828−7848.

(3) Madurantakam, P. A.; Cost, C. P.; Simpson, D. G.; Bowlin, G. L. Science of Nanofibrous Scaffold Fabrication: Strategies for Next Generation Tissue-Engineering Scaffolds. *Nanomedicine* **2009**, *4*, 193−206.

(4) Kim, S. E.; Wang, J.; Jordan, A. M.; Korley, L. T. J.; Baer, E.; Pokorski, J. K. Surface Modification of Melt Extruded Poly(ε-caprolactone) Nanofibers: Toward a New Scalable Biomaterial Scaffold. *ACS Macro Lett.* **2014**, *3*, 585−589.

(5) Stevens, M. M. Biomaterials for Bone Tissue Engineering. *Mater. Today* **2008**, *11*, 18−25.

(6) Obrien, F. J. Biomaterials & Scaffolds for Tissue Engineering. *Mater. Today* **2011**, *14*, 88−95.

(7) Grafahrend, D.; Heffels, K.-H.; Beer, M. V.; Gasteier, P.; MOller, M.; Boehm, G.; Dalton, P. D.; Groll, J. Degradable Polyester Scaffolds with Controlled Surface Chemistry Combining Minimal Protein Adsorption with Specific Bioactivation. *Nat. Mater.* **2011**, *10*, 67−73.

(8) Rezwan, K.; Chen, Q. Z.; Blaker, J. J.; Boccaccini, A. R. Biodegradable and Bioactive Porous Polymer/Inorganic Composite Scaffolds for Bone Tssue Engineering. *Biomater.* **2006**, *27*, 3413−3431.

(9) Hersel, U.; Dahmen, C.; Kessler, H. RGD Modified Polymers: Biomaterials for Stimulated Cell Adhesion and Beyond. *Biomaterials* **2003**, *24*, 4385−4415.

(10) Ferreira, A. M.; Gentile, P.; Chiono, V.; Ciardelli, G. Collagen for Bone Tissue Regeneration. *Acta Biomater.* **2012**, *8*, 3191−3200.

(11) Ramiro-Gutiérrez, M. L.; Will, J.; Boccaccini, A. R.; Díaz-Cuenca, A. Reticulated Bioactive Scaffolds with Improved Textural Properties for Bone Tissue Engineering: Nanostructured Surfaces and Porosity. *J. Biomed. Mater. Res., Part A* **2014**, *102*, 2982−2992.

(12) Ma, P. X. Biomimetic Materials for Tissue Engineering. *Adv. Drug Delivery Rev.* **2008**, *60*, 184−198.

(13) Jang, J. H.; Castano, O.; Kim, H. W. Electrospun Materials as Potential Platforms for Bone Tissue Engineering. *Adv. Drug Delivery Rev.* **2009**, *61*, 1065−1083.

(14) Lee, J. H.; Park, J. H.; Yun, Y. R.; Jang, J. H.; Lee, E. J.; Chrzanowski, W.; Wall, I. B.; Kim, H. W. Tethering Bi-functional Protein onto Mineralized Polymer Scaffolds to Regulate Mesenchymal Stem Cell Behaviors for Bone Regeneration. *J. Mater. Chem. B* **2013**, *1*, 2731−2741.

(15) Lee, J. H.; Park, J. H.; Fiqi, A. E.; Kim, J. H.; Yun, Y. R.; Jang, J. H.; Han, C. M.; Lee, E. J.; Kim, H. W. Biointerface Control of Electrospun Fiber Scaffolds for Bone Regeneration: Engineered Protein link to Mineralized Surface. *Acta Biomater.* **2014**, *10*, 2750−2761.

(16) Wang, P.; Zhao, L.; Liu, J.; Weir, M. D.; Zhou, X.; Xu, H. H. K. Bone Tissue Engineering via Nanostructured Calcium Phosphate Biomaterials and Stem Cells. *Bone Res.* **2014**, *2*, 14017.

(17) Yoo, H. S.; Kim, T. G.; Park, T. G. Surface-functionalized Electrospun Nanofibers for Tissue Engineering and DrugDelivery. *Adv. Drug Delivery Rev.* **2009**, *61*, 1033−1042.

(18) Murphy, W. L.; McDevitt, T. C.; Engler, A. J. Materials as Stem Cell Regulators. *Nat. Mater.* **2014**, *13*, 547−557.

(19) Kshitiz; Park, J.; Kim, P.; Helen, W.; Engler, A. J.; Levchenko, A.; Kim, D. H. Control of Stem Cell Fate andFunction by Engineering Physical Microenvironments. *Inter. Bol. (Camb)* **2012**, *4*, 1008−1018.

(20) Engler, A. J.; Sen, S.; Sweeney, H. L.; Discher, D. E. Matrix Elasticity Directs Stem Cell Lineage Specification. *Cell* **2006**, *126*, 677−689.

(21) Carbone, E. J.; Jiang, T.; Nelson, C.; Henry, N.; Lo, K. W. H. Small Molecule Delivery Through Nanofibrous Scaffolds for Musculoskeletal Regenerative Engineering. *Nanomed. Nanotechnol. Biol. Med.* **2014**, *10*, 1691−1699.

(22) Phipps, M. C.; Xu, Y.; Bellis, S. L. Delivery of Platelet-derived GrowthFactor as a Chemotactic Factor for Mesenchymal Stem Cells by Bone-mimetic Electrospun Scaffolds. *PLoS One* **2012**, *7*, e40831.

(23) El-Fiqi, A.; Kim, J. H.; Kim, H. W. Osteogenic Fibrous Scaffolds of Biopolymer/Mesoporous Bioactive Glass Nanocarriers with Excellent Bioactivity and Long-Term Delivery of Osteogenic Drug. *ACS Appl. Mater. Interface* **2015**, *7*, 1140−1152.

(24) Kang, M. S.; Kim, J. H.; Singh, R. K.; Kim, H. W. Therapeutic-Designed Electrospun Bone Scaffolds: Mesoporous Bioactive Nanocarriers in Hollow Fiber Composites to Sequentially Deliver Dual Growth Factors. *Acta Biomater* **2015**, *16*, 103−116.

(25) Meng, J.; Xiao, B.; Zhang, Y.; Liu, J.; Xue, H.; Lei, J.; Kong, H.; Huang, Y.; Jin, Z.; Gu, N.; Xu, H. Super-paramagnetic Responsive Nanofibrous Scaffolds under Static Magnetic Field Enhance Osteogenesis for Bone Repair in Vivo. *Sci. Rep.* **2013**, *3*, 2655.

(26) Holzwarth, J. M.; Ma, P. X. Biomimetic Nanofibrous Scaffolds for Bone Tissue Engineering. *Biomaterials* **2011**, *32*, 9622−9629.

(27) Martins, A.; Araújo, J. V.; Reis, R. L.; Neves, N. M. Electrospun Nanostructured Scaffolds for Tissue Engineering Applications. *Nanomedicine* **2007**, *2*, 929−942.

(28) Yu, H. S.; Jang, J. H.; Kim, T. I.; Lee, H. H.; Kim, H. W. Apatite Mineralized Polycaprolactone Nanofibrous Web as a Bone Tissue Regeneration Substrate. *J. Biomed. Mater. Res., Part A* **2009**, *88A*, 747−54.

DOI: 10.1021/acsami.5b00692
ACS Appl. Mater. Interfaces 2015, 7, 8088−8098

(29) Hong, S. J.; Yu, H. S.; Kim, H. W. Tissue Engineering Polymeric Microcarriers with Macroporous Morphology and Bone-Bioactive Surface. *Macromol. Biosci.* **2009**, *9*, 639−645.
(30) Singh, R. K.; Kim, T. H.; Kim, J. J.; Lee, E. J.; Knowles, J. C.; Kim, H. W. Mesoporous Silica Tubular Nanocarriers for the Delivery of Therapeutic Molecules. *RSC Adv.* **2013**, *3*, 8692−8704.
(31) Singh, R. K.; Patel, K. D.; Lee, J. H.; Lee, E. J.; Kim, J.-H.; Kim, T. H.; Kim, H.-W. Potential of Magnetic Nanofiber Scaffolds with Mechanical and Biological Properties Applicable for Bone Regeneration. *PLoS One* **2014**, *9*, e91584.
(32) Patel, K. D.; El-Fiqi, A.; Lee, H.-Y.; Singh, R. K.; Kim, D.-Ae; Lee, H.-H.; Kim, H.-W. Chitosan−Nanobioactive Glass Electrophoretic Coatings with Bone Regenerative and Drug Delivering Potential. *J. Mater. Chem.* **2012**, *22*, 24945−24956.
(33) Singh, R. K.; Patel, K. D.; El-Fiqi, A. M.; Kim, H. W. A Novel Preparation of Magnetic Hydroxyapatite Nanotubes. *Mater. Lett.* **2012**, *75*, 130−133.
(34) Kweon, H. Y.; Yoo, M. K.; Park, I. K.; Kim, T. H.; Lee, H. S.; Oh, J. S.; Akaike, T.; Cho, C. S. A Novel Degradable Polycaprolactone Networks for Tissue Engineering. *Biomaterials* **2003**, *24*, 801−808.
(35) Singh, R. K.; Kim, T.-H.; Patel, K. D.; Knowles, J. C.; Kim, H.-W. Biocompatible Magnetite Nanoparticles with Varying Silica-Coating Layer for use in Biomedicine: Physicochemical and Magnetic Properties, and Cellular Compatibility. *J. Biomed. Mater. Res., Part A* **2012**, *100A*, 1734−1742.
(36) Stevens, M. M.; George, J. H. Exploring and Engineering the Cell Surface Interface. *Science* **2005**, *310*, 1135−1138.
(37) Holzwarth, J. M.; Ma, P. X. Biomimetic Nanofibrous Scaffolds for Bone Tissue Engineering. *Biomaterials* **2011**, *32*, 9622−9629.
(38) Ingavle, G. C.; Leach, J. K. Advancements in Electrospinning of Polymeric Nanofibrous Scaffolds for Tissue Engineering. *Tissue Eng. B* **2014**, *20*, 277−293.
(39) Hodgkinson, T.; Yuan, X.-F.; Bayat, A. Electrospun Silk Fibroin Fiber Diameter Influences In Vitro Dermal Fibroblast Behavior and Promotes Healing of Ex Vivo Wound Models. *J. Tissue Eng.* **2014**, *5*, 2041731414551661.
(40) Beachley, V.; Kasyanov, V.; Nagy-Mehesz, A.; Norris, R.; Ozolanta, I.; Kalejs, M.; Stradins, P.; Baptista, L.; da Silva, K.; Grainjero, J.; Wen, X.; Mironov, V. The Fusion of Tissue Spheroids Attached to Pre-stretched Electrospun Polyurethane Scaffolds. *J. Tissue Eng.* **2014**, *5*, 2041731414556561.
(41) Lin, H.-M.; Lin, Y.-H.; Hsu, F.-Y. Preparation and Characterization of Mesoporous Bioactive Glass/Polycaprolactone Nanofibrous Matrix for Bone Tissues Engineering. *J. Mater. Sci. Mater. Med.* **2012**, *11*, 2619−2622.
(42) Hou, Z.; Li, X.; Li, C.; Dai, Y.; Ma, P.; Zhang, X.; Kang, X.; Cheng, Z.; Lin, J. Electrospun Upconversion Composite Fibers as Dual Drugs Delivery System with Individual Release Properties. *Langmuir* **2013**, *30*, 9473−9482.
(43) Best, S.; Porter, A.; Thian, E.; Huang, J. Bioceramics: Past, Present and for the Future. *J. Eur. Ceram. Soc.* **2008**, *28*, 1319−1327.
(44) Jaiswal, A. K.; Chhabra, H.; Soni, V. P.; Bellare, J. R. Enhanced Mechanical Strength and Biocompatibility of Electrospun Polycaprolactone-gelatin Scaffold with Surface Deposited Nano-Hydroxyapatite. *Mater. Sci. Eng., C* **2013**, *13*, 2376−2385.
(45) Francis, L.; Meng, D.; Knowles, J. C.; Roy, I.; Boccaccini, A. R. Multi-functional P(3HB) Microsphere/45S5 Bioglass-based Composite Scaffolds for Bone Tissue Engineering. *Acta Biomater.* **2010**, *6*, 2773−2786.
(46) Gaharwar, A. K.; Dammu, S. A.; Canter, J. M.; Wu, C. J.; Schmidt, G. Highly Extensible, Tough, and Elastomeric Nanocomposite Hydrogels from Poly(ethylene glycol) and Hydroxyapatite Nanoparticles. *Biomacromolecules* **2011**, *12*, 1641−1650.
(47) Yang, F.; Wolke, J.; Jansen, J. Biomimetic Calcium Phosphate Coating on Electrospun Poly(ε-caprolactone) Scaffolds for Bone Tissue Engineering. *Chem. Eng. J.* **2008**, *137*, 154−161.
(48) Seyedjafari, E.; Soleimani, M.; Ghaemi, N.; Shabani, I. Nanohydroxyapatite-coated Electrospun Poly(l-lactide) Nanofibers Enhance Osteogenic Differentiation of Stem Cells and Induce Ectopic Bone Formation. *Biomacromolecules* **2010**, *11*, 3118−3125.
(49) Singh, R. K.; Patel, K. D.; Kim, J. J.; Kim, T. H.; Kim, J. H.; Shin, U. S.; Lee, E. J.; Knowles, J. C.; Kim, H. W. Multifunctional Hybrid Nanocarrier: Magnetic CNTs Ensheathed with Mesoporous Silica for Drug Delivery and Imaging System. *ACS Appl. Mater. Interfaces* **2014**, *6*, 2201−2208.
(50) Padial-Molina, M.; Galindo-Moreno, P.; Fernández-Barbero, J. E.; O'Valle, F.; Jódar-Reyes, A. B.; Ortega-Vinuesa, J. L.; Torregrosa, P. J. R. Role of Wettability and Nanoroughness on Interactions between Osteoblast and Modified Silicon Surfaces. *Acta Biomater.* **2011**, *7*, 771−778.
(51) Yun, H. S.; Kim, S. H.; Khang, D. W.; Choi, J. I.; Kim, H. H.; Kang, M. Biomimetic Component Coating on 3D Scaffolds using High Bioactivity of Mesoporous Bioactive Ceramics. *J. Int. J. Nanomed.* **2011**, *6*, 2521−2531.
(52) Watt, F. M.; Huck, W. T. S. Role of the Extracellular Matrix in Regulating Stem Cell Fate. *Nat. Rev. Mol. Cell Biol.* **2013**, *14*, 467−473.
(53) Wang, Y. K.; Chen, C. S. Cell Adhesion and Mechanical Stimulation in the Regulation of Mesenchymal Stem Cell Differentiation. *J. Cell Mol. Med.* **2013**, *17*, 823−832.
(54) Isaac, J.; Nohra, J.; Lao, J.; Jallot, E.; Nedelec, J. M.; Berdal, A.; Sautier, J. M. Effects of Strontium-doped Bioactive Glass on the Differentiation of Cultured Osteogenic Cells. *Eur. Cell Mater.* **2011**, *21*, 130−143.
(55) Golub, E. E.; Boesze-Battaglia, K. The Role of Alkaline Phosphatase in Mineralization. *Curr. Opin. Orthop.* **2007**, *18*, 444−448.
(56) Aubin, J. E. Bone Stem Cells. *J. Cell Biochem. Suppl.* **1998**, *30*−*31*, 73−82.
(57) Thurner, P. J.; Chen, C. G.; Ionova-Martin, S.; Sun, L.; Harman, A.; Porter, A.; Ager, J. W., 3rd; Ritchie, R. O.; Alliston, T. Osteopontin Deficiency Increases Bone Fragility but Preserves Bone Mass. *Bone* **2010**, *46*, 1564−1573.
(58) Alvarez Perez, M. A.; Guarino, V.; Cirillo, V.; Ambrosio, L. In Vitro Mineralization and Bone Osteogenesis in Poly(ε-caprolactone)/gelatin Nanofibers. *J. Biomed. Mater. Res., Part A* **2012**, *100*, 3008−3019.

DOI: 10.1021/acsami.5b00692
ACS Appl. Mater. Interfaces 2015, 7, 8088−8098